Inorganic Chemistry

Article

pubs.acs.org/IC

A Tripodal Ruthenium–Gadolinium Metallostar as a Potential $\alpha_v\beta_3$ Integrin Specific Bimodal Imaging Contrast Agent

Peter Verwilst,[†,∥] Svetlana V. Eliseeva,[†,‡,§] Luce Vander Elst,[▽] Carmen Burtea,[▽] Sophie Laurent,[▽] Stéphane Petoud,[‡] Robert N. Muller,[▽,#] Tatjana N. Parac-Vogt,[†] and Wim M. De Borggraeve*[,†]

[†]University of Leuven, Department of Chemistry, Celestijnenlaan 200F–P.O. Box 2404, B-3001 Heverlee, Belgium

[‡]Centre de Biophysique Moléculaire, UPR 4301 CNRS, Rue Charles Sadron, 45071 Orléans Cedex 2, France

[§]Le STUDIUM, Institute for Advanced Studies, Orléans & Tours, France

[▽]NMR and Molecular Imaging Laboratory, Department of General, Organic and Biomedical Chemistry, University of Mons-Hainaut, B-7000 Mons, Belgium

[#]Center for Microscopy and Molecular Imaging, Rue Adrienne Bolland 8, B-6041 Charleroi, Belgium

Supporting Information

ABSTRACT: Gd^{III}-containing *metallostar* contrast agents are gaining increased attention, because their architecture allows for a slower tumbling rate, which, in turn, results in larger relaxivities. So far, these *metallostars* find possible applications as blood pool contrast agents. In this work, the first example of a tissue-selective *metallostar* contrast agent is described. This RGD-peptide decorated $Ru^{II}(Gd^{III})_3$ *metallostar* is synthesized as an $\alpha_v\beta_3$-integrin specific contrast agent, with possible applications in the detection of atherosclerotic plaques and tumor angiogenesis. The contrast agent showed a relaxivity of 9.65 s^{-1} mM^{-1}, which represents an increase of 170%, compared to a low-molecular-weight analogue, because of a decreased tumbling rate (τ_R = 470 ps). The presence of the MLCT band (absorption 375–500 nm, emission 525–850 nm) of the central $Ru^{II}(Ph\text{-}Phen)_3$-based complex grants the *metallostar* attractive luminescent properties. The ^{3}MLCT emission is characterized by a quantum yield of 4.69% and a lifetime of 804 ns, which makes it an interesting candidate for time-gated luminescence imaging. The potential application as a selective MRI contrast agent for $\alpha_v\beta_3$-integrin expressing tissues is shown by an *in vitro* relaxometric analysis, as well as an *in vitro* T_1-weighted MR image.

INTRODUCTION

The use of Gd^{III}-containing *metallostars* (complexes in which a single branching site has several metallated arms)[1] as magnetic resonance imaging (MRI) contrast agents is gaining attention, because of their improved relaxometric behavior.[2−10] Furthermore, it has been shown that Ru^{II}–Gd^{III}-based *metallostars* can potentially be used as contrast agents for bimodal imaging,[8,9] because of the presence of an intense red to near-infrared luminescence that results from the relatively long-lived metal-to-ligand charge transfer (MLCT) states of the Ru^{II} center.[11,12] These contrast agents combine the good spatial resolution of the MRI technique (which is limited by low sensitivity)[13] with the high-resolution images that can be obtained from thin tissue samples or cells with luminescence-based imaging,[14−16] leading to complementary information with a molecule possessing an identical biodistribution.[16,17] Several research groups are presently involved in the field of bimodal optical/MRI imaging,[18] and in addition to *metallostars*, other compounds have been suggested as potential contrast agents.[19,20]

So far, these *metallostar* contrast agents have been mainly designed as blood pool contrast agents via interactions with human serum albumin (HSA) and do not exhibit specificity for certain cells or tissues.[5,6,8−10]

RGD-bearing low-molecular-weight contrast agents, exhibiting a selectivity for $\alpha_v\beta_3$ integrins, were previously reported.[21−23] The integrin is expressed on activated endothelial cells and plays a key role in the formation of atherosclerotic plaques[24] and tumor neovascularization.[25] It has been shown that the binding of an RGD-peptide- or RGD-peptidomimetic-decorated MRI contrast agent to the $\alpha_v\beta_3$-integrin causes a local immobilization of the agent, resulting in a better contrast and thus allowing the detection of tissues expressing this integrin.[21,22,26,27]

In this work, we report the synthesis and characterization of a novel Ru^{II}–Gd^{III} *metallostar* contrast agent, exhibiting selectivity toward $\alpha_v\beta_3$ integrins. This contrast agent combines the selectivity of the RGD peptide with luminescent properties and an improved relaxivity, because of the heterometallic Ru^{II}–Gd^{III} *metallostar* architecture. An analogous Ru^{II}–La^{III} *metallostar* was synthesized to allow the characterization of the intermediate complexes by ^{1}H NMR.

RESULTS AND DISCUSSION

Synthesis of Complexes. The 1,7-*tert*-butyl acety-substituted 1,4,7,10-tetraaza cyclododecane (**1**)[28] was mono-*N*-alkylated with 2-bromo-*N*-propargyl acetamide (**2**)[29] in the presence of K_2CO_3 in acetonitrile (ACN), resulting in the trisubstituted cyclen derivative (**3**). This cyclen derivative was further *N*-alkylated with a phenantroline analogue **5** (resulting from the reaction of aniline **4**[9] with bromoacetyl bromide in

Received: April 6, 2012
Published: May 14, 2012

   dx.doi.org/10.1021/ic300717m | Inorg. Chem. 2012, 51, 6405–6411

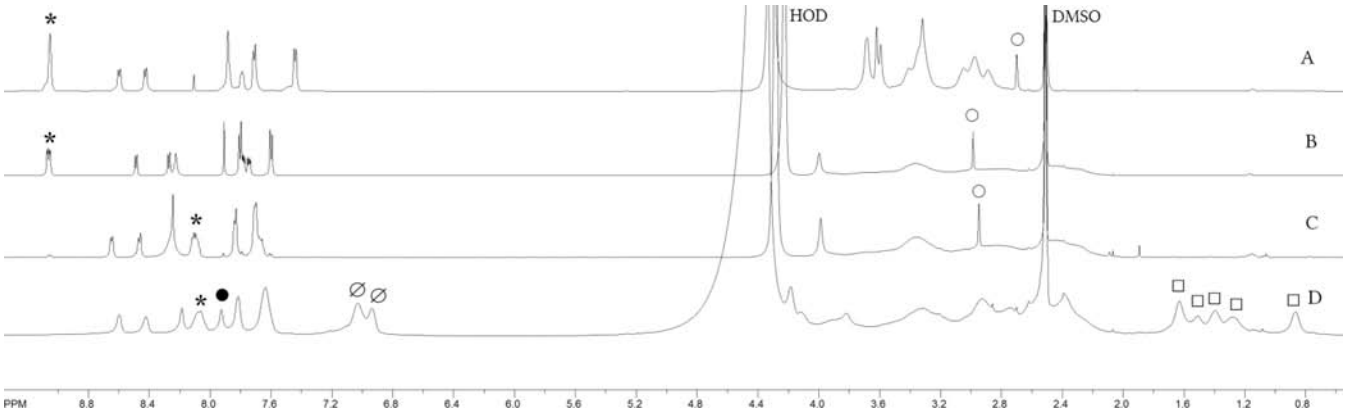

Figure 1. Stacked ^{1}H NMR spectra of the La^{III} complexes (in 2/1 DMSO-d_6/D_2O): (A) **6**, (B) **La.6**, (C) **Ru(La.6)$_3$**, and (D) **Ru(La.8)$_3$**. (Legend: (*) phenantroline C2-*H* and C9-*H*, (○) alkyne-*H*, (●) triazole C5-*H*, (⌀) phenylalanine aromatic C-*H*, (□) lysine β-, γ-, and δ-CH_2, arginine β- and γ-CH_2.).

Scheme 1. Synthesis of the Ru^{II}–Ln^{III} Complexes Ru(Ln.8)$_3$ (Ln = La, Gd)

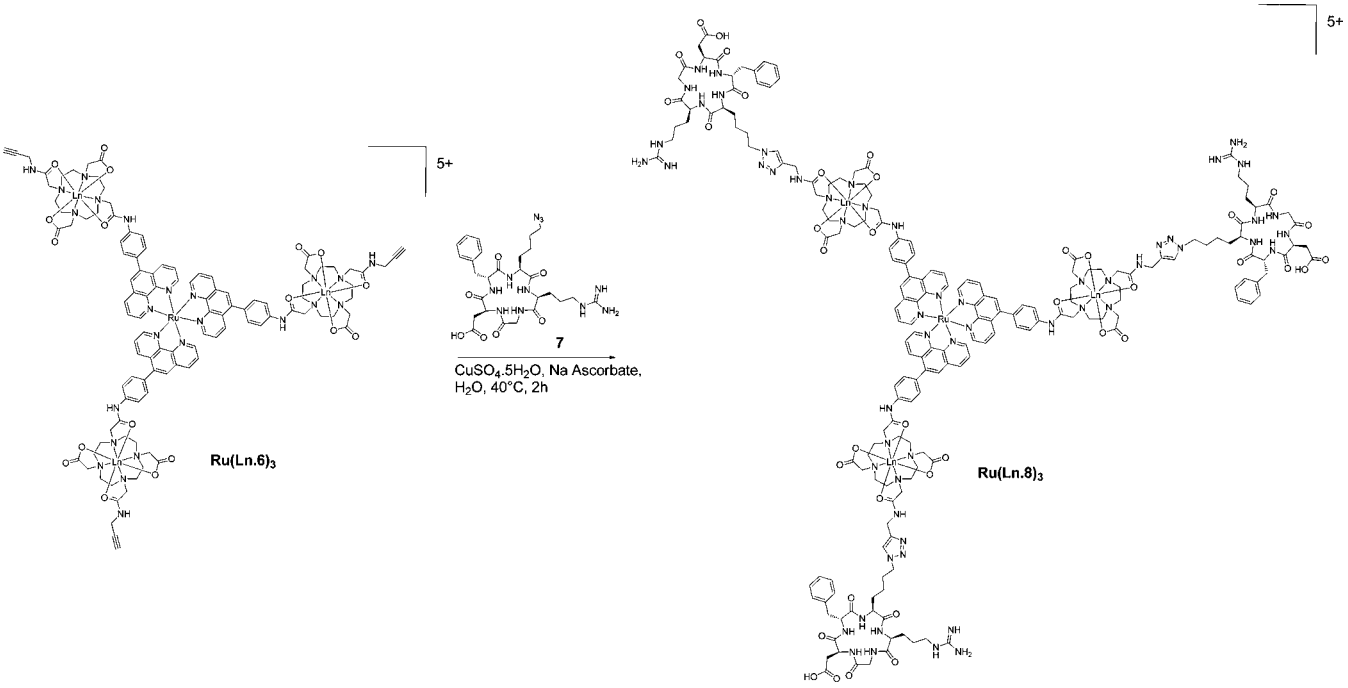

dichloromethane (DCM)) in the presence of K_2CO_3 in ACN, yielding the propargyl-bearing ligand (**6**) after deprotection with trifluoroacetic acid (TFA) in DCM (see Scheme S1 in the Supporting Information).

The lanthanide complexes **Ln.6** (Ln = La, Gd) were obtained by adding a slight excess of the corresponding lanthanide trichloride hydrate to an aqueous solution of the ligand. The solution was neutralized by KOH and stirred overnight at 60 °C (see Scheme S2 in the Supporting Information). Subsequently, any free lanthanide ions were removed by treatment with Chelex 100 beads. The solution was checked with an arsenazo indicator solution, which confirmed the complete removal of free lanthanide ions.[30] The successful synthesis was confirmed by the ^{1}H NMR of the La^{III} complex (Figure 1), which shows a broadening of the DOTA signals in the aliphatic region, whereas the propagylic signals were not broadened. Some (relatively small) shifts of the propargylic and aromatic signals were observed as the ligand adopts a cuplike conformation upon chelating the central La^{III} ion. HPLC/MS and IR further confirmed the successful synthesis of **Ln.6**. The complexes were reacted with $RuCl_3$ in a 1/1 mixture of water and ethanol at 78 °C, resulting in an intense orange solution of the Ru^{II}–Ln^{III} complexes **Ru(Ln.6)$_3$** (see Scheme S3 in the Supporting Information). Here, the ^{1}H NMR of **Ru(La.6)$_3$** revealed major shifts in the aromatic region, particularly the signal of the protons that come into closest contact with the Ru^{II} center shifted nearly 1 ppm unit (Figure 1). No changes in the aliphatic region were observed. HPLC/MS and IR further confirmed the successful synthesis. Finally, the complexes were decorated with an azide-bearing RGD pentapeptide (**7**)[31] using the click reaction,[32,33] resulting in the RGD bearing Ru^{II}–Ln^{III} complexes **Ru(Ln.8)$_3$** (Scheme 1). In this case, the ^{1}H NMR of **Ru(La.8)$_3$** showed the appearance of a triazole signal, and the disappearance of the alkyne signal, indicating a successful click reaction. This observation is further confirmed by the appearance of the characteristic signals of the peptide side-

dx.doi.org/10.1021/ic300717m | *Inorg. Chem.* 2012, 51, 6405–6411

chains (Figure 1). Again, the successful synthesis was confirmed by high-performance liquid chromatography/mass spectroscopy (HPLC/MS) and infrared (IR) spectroscopy, as well as the photophysical properties of the final **Ru(Gd.8)$_3$** complex.

Relaxometric Studies. The water proton relaxivity (r_1), which is defined as the paramagnetic longitudinal relaxation rate of a 1 mM solution of Gd^{III}, is characterized by four parameters: q, the number of water molecules in the first coordination sphere of Gd^{III}; τ_M, the residence time of the coordinated water molecule(s); τ_{S0}, the Gd^{III} electronic relaxation correlation time at zero field; and τ_R, the rotational correlation time.

The residence time of the coordinated water molecule can be determined from the analysis of the temperature dependence of the transverse relaxation rate of the ^{17}O resonance of bulk water in solutions of gadolinium complexes.[34−37] A theoretical treatment of the experimental data[34,35,38,39] (Figure 2) was

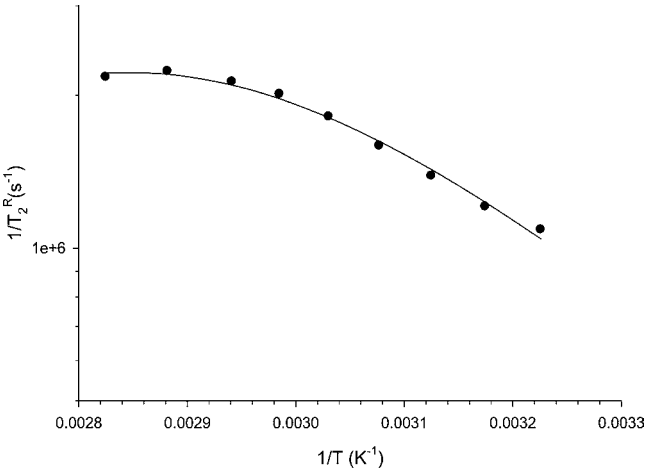

Figure 2. Temperature dependence of the reduced transverse relaxation rate of ^{17}O at 11.75 T (7.7 mM **Ru(Gd.8)$_3$**).

performed assuming the presence of one water molecule in the first coordination sphere of Gd^{III} (Table 1). The value of $A/\hbar$,

Table 1. Parameters Obtained by the Theoretical Adjustment of the ^{17}O Transverse Relaxation Rates versus the Reciprocal of the Temperature of Ru(Gd.8)$_3$

parameter	value
τ_M^{310}	779 ± 47 ns
$\Delta H^{\ddagger}$	34.43 ± 0.08 kJ mol^{-1}
$\Delta S^{\ddagger}$	−17.1 ± 0.25 J mol^{-1}K^{-1}

the hyperfine coupling constant between the oxygen nucleus of the bound water and the Gd^{III} ion was fixed to -3.8×10^6 rad s^{-1}.[4,40] This resulted in the determination of the following parameters: τ_M; $\Delta H^{\ddagger}$ and $\Delta S^{\ddagger}$, the enthalpy and entropy of the water exchange process, respectively; B, related to the mean square of the zero-field splitting energy ($B = 2.4\Delta^2$); τ_V, the correlation time modulating the electronic relaxation of Gd^{III} and E_V, the activation energy related to τ_V.

The τ_M value obtained by this theoretical treatment is comparable to τ_M values of other contrast agents, in which the Gd^{III} ion is surrounded by two amide bonds.[41] The data obtained show that the exchange rate is in the slow to intermediate regime in the 310−354 K range and, therefore, the fitted parameters related to the electronic relaxation were not considered.

The **Ru(Gd.8)$_3$** complex was subsequently investigated by proton nuclear magnetic relaxation dispersion (NMRD) measurements in water at 310 K in order to determine the remaining two characteristic parameters. The possibility of stacking interactions was excluded by recording the NMRD profile for two different concentrations (1.52 mM Gd^{III} and 0.85 mM Gd^{III}), revealing an identical profile (see Figure 3).

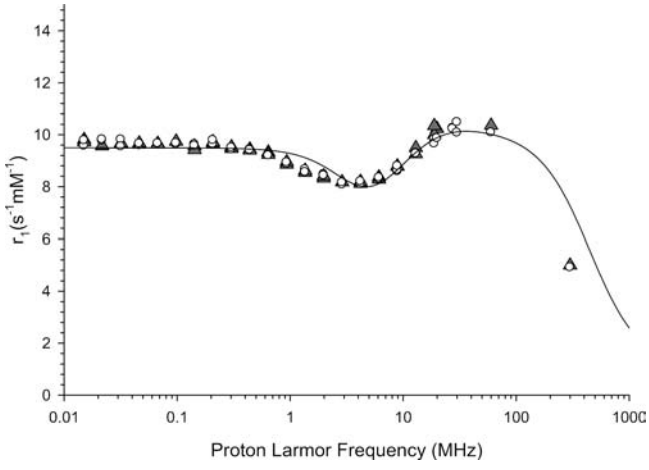

Figure 3. NMRD relaxivity profile of **Ru(Gd.8)$_3$** for two different concentrations (1.52 mM (circles) and 0.85 mM (triangles)) at 310 K. The line corresponds to the theoretical fitting of the data points.

The theoretical adjustments of the NMRD profile takes into account the inner-sphere[42,43] and outer-sphere[44] contributions to the paramagnetic relaxation rate. Some parameters were fixed during this fitting procedure: q, the number of water molecules in the first coordination sphere of Gd^{III} ($q = 1$); d, the distance of closest approach ($d = 0.36$ nm); D, the relative diffusion constant ($D = 3.3 \times 10^{-9}$ m^2 s^{-1})[45] and r, the distance between the Gd^{III} ion and the proton nuclei of water ($r = 0.31$ nm). The residence time of the coordinated water molecule (τ_M) was allowed to fluctuate between 800 and 900 ns. The results of this fitting, compared with a small molecular weight contrast agent bearing the same RGD peptide (GdL-RGD)[23] and GdDOTA are reported in Table 2.

As can be seen from Table 2, the *metallostar* architecture of **Ru(Gd.8)$_3$** induces an important advantage over the low-molecular-weight analogue[23] as can be observed from the 170% relative increase in relaxivity at 20 MHz and 310 K and a 275% relative increase versus GdDOTA.[38] However, this increase is

Table 2. Parameters Obtained by the Theoretical Fitting of the Proton NMRD Data in Water at 310 K of Ru(Gd.8)$_3$, Compared to Literature Values

	Value		
parameter	**Ru(Gd.8)$_3$**	GdL-RGD[a]	GdDOTA[b]
τ_m^{310} (ns)	850 ± 1	343 ± 10	122 ± 10
τ_R^{310} (ps)	469 ± 11	112 ± 4	53 ± 1
τ_{SO}^{310} (ps)	111 ± 1	122 ± 4	404 ± 24
τ_V^{310} (ps)	36 ± 1	16 ± 1	7 ± 1
r_1 (s^{-1} mM^{-1})[c]	9.65 ± 0.08	5.7	3.5

[a]From ref 23. [b]From ref 38. [c]At 20 MHz and 310 K.

dx.doi.org/10.1021/ic300717m | Inorg. Chem. 2012, 51, 6405−6411

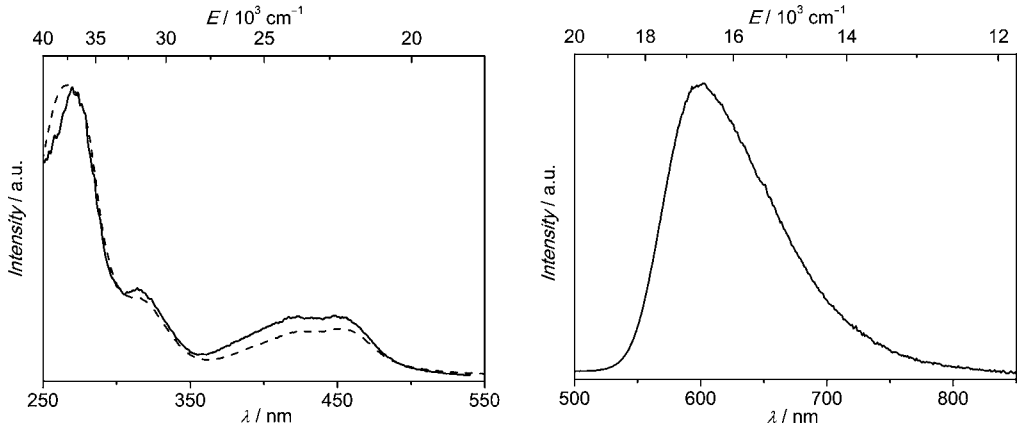

Figure 4. (Left) Excitation (solid line, λ_{em} = 600 nm) and superimposed absorption (dash line) spectra, and (right) emission spectra (λ_{ex} = 450 nm) of 2 × 10^{-5} M solutions of **Ru(Gd.8)$_3$** peptide in H_2O at room temperature.

limited by the slow water exchange, because of the amide bonds. The fitted rotational correlation time (τ_R) value is in good agreement with the expected value considering the size of the molecule (a value of $\tau_{R(metallostar)}$ = 432 ps was calculated by the simple equation: τ_R(Gd-DOTA) × MW(metallostar)/MW(Gd-DOTA)). This fitted value of τ_R shows the absence of internal motion as expected from the highly conjugated structure of the compound. The interaction of the complex **Ru(Gd.8)$_3$** with HSA was determined,[46] revealing no significant binding interactions (see Figure S1 in the Supporting Information), and thus allowing the peptide to bind its target without any interference with HSA. The increase in observed relaxation rate of the NMRD profile of **Ru(Gd.8)$_3$** in a 4% HSA solution is caused by the increased viscosity of this HSA solution, rather than a specific interaction (see Figure S2 in the Supporting Information).

Photophysical Properties. The electronic absorption spectrum of **Ru(Gd.8)$_3$** displays bands due to d→π^* metal-to-ligand charge transfer (^{1}MLCT) transitions in the visible range at 375−500 nm (Figure 4). In addition, an intense band in the UV corresponding to the ligand $\pi\rightarrow\pi^*$ transitions is present with an apparent maximum at 270 nm. The shoulder at 320 nm can be attributed to Ru^{II} centered d→d transitions.[11,12] The excitation spectrum of the **Ru(Gd.8)$_3$** complex, recorded by monitoring the emission at 600 nm closely resembles the absorption spectrum (Figure 4). Upon excitation into the ^{1}MLCT band at 450 nm, the complex exhibits a bright red luminescence in the visible range (525−850 nm, centered at 600 nm, Figure 4), further extending to the near-infrared range up to 1200 nm. The quantum yield of the visible emission was determined using an absolute method and was found to be 4.69% ± 0.05%. The lifetime of **Ru(Gd.8)$_3$** equal to 804 ± 6 ns. In general, the photophysical parameters of **Ru(Gd.8)$_3$** are in the range of other luminescent Ru^{II} complexes.[11,12]

In order to test the potential use of **Ru(Gd.8)$_3$** for optical imaging, a 10^{-5} M solution of the complex was placed into a test capillary and visualized using a macroscope (Figure 5). The luminescence signal could be detected not only in the visible but also in the near-infrared range with a good signal-to-noise ratio.

Biological Data. *In Vitro Validation of the Interaction of **Ru(Gd.8)$_3$** with $\alpha_v\beta_3$ Integrin by Proton Relaxometry.* **Ru(Gd.8)$_3$** was evaluated on Jurkat T cells to confirm the preservation of its affinity for integrins. The proton longitudinal relaxation time, T_1, was determined for a sample containing

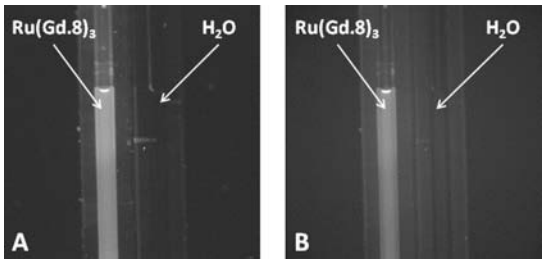

Figure 5. Luminescence images of 10^{-5} M aqueous solutions of **Ru(Gd.8)$_3$** in capillaries: (A) visible emission (λ_{ex} = 482 nm, BP = 35 and λ_{em} = 607 nm, BP = 75; exposure time 100 ms) and (B) near-infrared emission (λ_{ex} = 447 nm, BP = 60 and λ_{em} = 770 nm, LP filter; exposure time 300 ms).

stimulated Jurkat T cells, which overexpress α_v integrins, and **Ru(Gd.8)$_3$**, as well as for a series of control samples at 300 MHz (7T) and 288 K. R_1^{Norm}, which is the difference between the relaxation rates in the presence and absence of a contrast agent, was determined. As can be seen from Figure 6, the proton longitudinal relaxation rate in the presence of **Ru(Gd.8)$_3$** and stimulated Jurkat T cells shows a significant increase in respect to the control samples, thus confirming the retained interaction of the RGD peptide with the integrins of the stimulated Jurkat T cells.

*In Vitro Validation of the Interaction of **Ru(Gd.8)$_3$** with $\alpha_v\beta_3$ Integrin by 7 T MRI.* A T_1 weighted MRI image at 288 K at a field of 7 T confirmed the observations of the proton relaxometry experiment. As can be seen from Figure 7, the most intense signal, leading to the most enhanced contrast with the background was observed for stimulated Jurkat T cells (overexpressing α_v integrins) in the presence of **Ru(Gd.8)$_3$** as a contrast agent (Figure 7, image 1).

■ CONCLUSIONS

A new tetranuclear heterobimetallic contrast agent is presented. This novel *metallostar* contrast agent, **Ru(Gd.8)$_3$** is decorated with three RGD peptides via the click reaction, enabling the detection of $\alpha_v\beta_3$-integrin expressing tissues. The contrast agent exhibits a relaxivity of 9.65 s^{-1} mM^{-1} at 20 MHz and 310 K, which represents a 170% improvement versus a previously published low-molecular-weight analogue (5.7 s^{-1} mM^{-1}) and a 275% improvement versus GdDOTA (3.5 s^{-1} mM^{-1}). This increased relaxivity is caused by the slow tumbling rate of this fairly large contrast agent (τ_R = 470 ps). Unfortunately, the

dx.doi.org/10.1021/ic300717m | Inorg. Chem. 2012, 51, 6405−6411

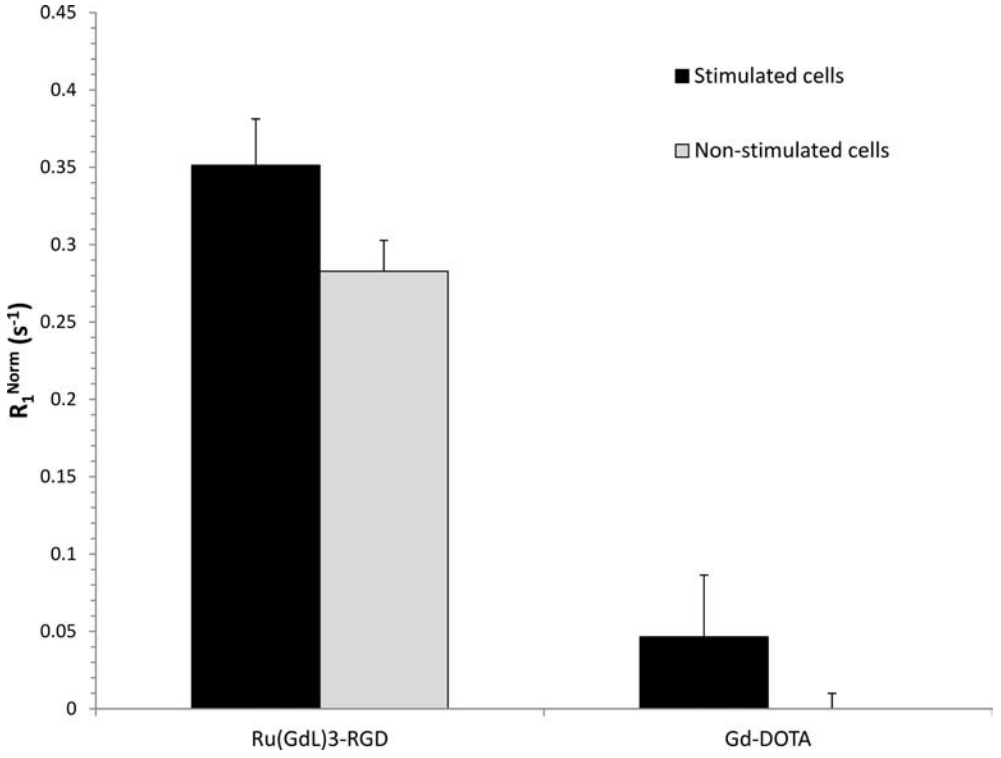

Figure 6. R_1^{Norm} of stimulated cells (black) and nonstimulated cells (gray) at 300 MHz and 288 K.

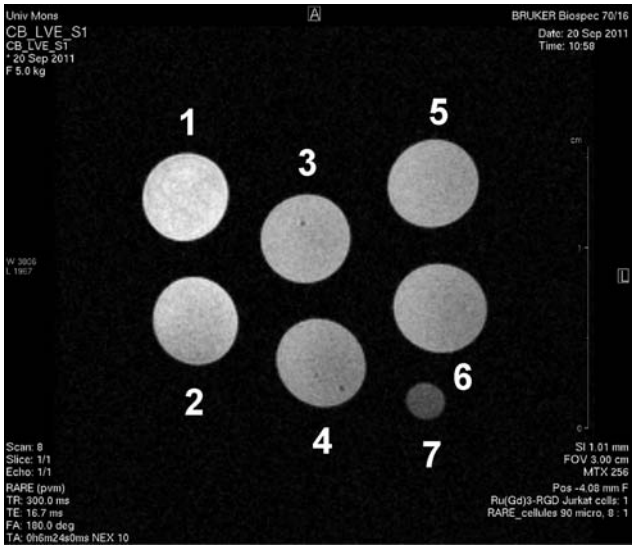

Figure 7. T_1-weighted MRI image of Jurkat T cells, incubated with **Ru(Gd.8)$_3$**, and a few control samples: (1) stimulated Jurkat T cells with **Ru(Gd.8)$_3$**; (2) nonstimulated Jurkat T cells with **Ru(Gd.8)$_3$**; (3) stimulated Jurkat T cells with GdDOTA, (4) nonstimulated Jurkat T cells with GdDOTA; (5) stimulated Jurkat T cells without contrast agent; (6) nonstimulated Jurkat T cells without contrast agent; and (7) phantom containing 50 μM GdDTPA (no cells).

decreased water exchange rate ($\tau_M \approx 850$ ns), caused by the presence of two amide bonds near the Gd^{III} center, limits the relaxivity value. However, the *in vitro* biological evaluation shows the potential of this contrast agent to detect $\alpha_v\beta_3$-integrin expressing cells, both by proton relaxometry and by MRI. Moreover, the *metallostar* **Ru(Gd.8)$_3$** exhibits a bright red luminescence with a quantum yield of 4.69% and a lifetime of 804 ns. The feasibility of using **Ru(Gd.8)$_3$** as imaging agent both in the visible and near-infrared ranges have been illustrated by luminescence macroscopy of its solution in a capillary. These properties make **Ru(Gd.8)$_3$** a promising candidate as a contrast agent for both luminescence and MRI detection of $\alpha_v\beta_3$-integrin-expressing tissues. The robustness of the click reaction in the modular pathway followed in the synthesis of this contrast agent could be further implemented, enabling the synthesis of new specific bimodal contrast agents.

EXPERIMENTAL SECTION

Materials. The azide-bearing RGD pentapeptide (**7**)[31] was purchased from SBS Genetech (Beijing, China). 1,7-*tert*-butyl acetyl 1,4,7,10-tetraaza cyclododecane (**1**),[28] 2-bromo-*N*-propargyl acetamide (**2**)[29] and [4-(1,10-phenanthrolin-5-yl)phenyl]amine (**4**)[9] were synthesized according to a literature procedure. All other reagents were obtained from Sigma–Aldrich (Bornem, Belgium), Acros (Geel, Belgium), or ABCR (Karlsruhe, Germany) and were used without further purification.

Synthesis. *Synthesis of **3**, **5**, **6**, **La.6**, **Gd.6**, **Ru(La.6)$_3$**, and **Ru(Gd.6)$_3$**.* See the Supporting Information.

*Synthesis of Ruthenium(II) tris-{lanthanum 2,2′-[4-(2-{[(1-{5-[(2S,5S,11S,14R)-5-(3-{[amino(imino)methyl]amino}propyl)-14-benzyl-11-(2-carboxyethyl)-3,6,9,12,15-pentaoxo-1,4,7,10,13-pentaazacyclopentadecan-2-yl]pentyl}-1H-1,2,3-triazol-4-yl)methyl]amino}-2-oxoethyl)-10-(2-oxo-2-{[4-(1,10-phenanthrolin-5-yl)phenyl]amino}ethyl)-1,4,7,10-tetraazacyclododecane-1,7-diyl]diacetate} Pentachloride (**Ru(La.8)$_3$**).* Thirty micromoles (30 μmol) of **Ru(La.6)$_3$** and 98 mg (150 μmol) of **7** were dissolved in 1 mL of deionized water. 0.1 mL of a 30 mM solution (3.0 μmol) of $CuSO_4 \cdot 5H_2O$, and 0.1 mL of a 60 mM solution of sodium ascorbate (6.0 μmol) were added and the solution was stirred for 4 h at 45 °C under an argon atmosphere. The solvent was removed by lyophilization and chromatographic purification (C18 silica; HPLC; Solvent A, H_2O + 0.1% HCOOH; Solvent B, ACN; 0% B →10% B, 5 min; 10% B → 30% B, 30 min) yielded the corresponding Ru^{II}–La^{III} complex **Ru(La.8)$_3$** as orange solid after lyophilization. Yield: 40%. HPLC: tr 22.75 min. Purity (215 nm): 95.91%. ^{1}H NMR (300 MHz, DMSO-d_6 + D_2O, ppm): δ 8.60 (d, J = 8.3 Hz, 3H), 8.41 (d, J = 8.0

dx.doi.org/10.1021/ic300717m | *Inorg. Chem.* 2012, 51, 6405–6411

Hz, 3H), 8.18 (s, 3H), 8.11−8.01 (m, 6H), 7.91 (s, 3H), 7.81 (d, J = 6.8 Hz, 6H), 7.70−7.57 (m, 12H), 7.17−6.87 (m, 15H), 4.05−2.26 (m, 120H), 1.70−1.23 (m, 24H), 0.90 (s, 6H). IR (neat): 3273, 1627, 1593, 1552 cm^{-1}. ESI-MS, $C_{192}H_{237}La_3N_{57}O_{39}Ru^{5+}$ $[M]^{5+}$, 1121 $[M+e]^{4+}$, 879 $[M]^{5+}$, 748 $[M+H]^{6+}$, 641 $[M+2H]^{7+}$, 561 $[M+3H]^{8+}$.

*Synthesis of Ruthenium(II) tris-{gadolinium 2,2′-[4-(2-{[(1-{5-[(2S,5S,11S,14R)-5-(3-{[amino(imino)methyl]amino}propyl)-14-benzyl-11-(2-carboxyethyl)-3,6,9,12,15-pentaoxo-1,4,7,10,13-pentaazacyclopentadecan-2-yl]pentyl}-1H-1,2,3-triazol-4-yl)methyl]amino}-2-oxoethyl)-10-(2-oxo-2-{[4-(1,10-phenanthrolin-5-yl)phenyl]amino}ethyl)-1,4,7,10-tetraazacyclododecane-1,7-diyl]diacetate} Pentachloride (**Ru(Gd.8)$_3$**).* See **Ru(La.8)$_3$** for experimental procedure. Yield: 43%. HPLC: tr 22.09 min. Purity (215 nm): 98.44%. IR (neat): 3254, 1627, 1598, 1551 cm^{-1}. ESI-MS, $C_{192}H_{237}Gd_3N_{57}O_{39}Ru^{5+}$ $[M]^{5+}$, 1136 $[M+e]^{4+}$, 908 $[M]^{5+}$, 757 $[M+H]^{6+}$, 649 $[M+2H]^{7+}$, 568 $[M+3H]^{8+}$.

Instruments. ^1H and ^{13}C spectra were recorded using a Bruker Avance 300 spectrometer (Bruker, Karlsruhe, Germany) operating at 300 MHz for ^1H and 75 MHz for ^{13}C or a Bruker Avance 400 spectrometer, operating at 100 MHz for ^{13}C. IR spectra were measured using a Bruker Alpha-T FT-IR spectrometer (Bruker, Ettlingen, Germany) and data were processed with opus 6.5q software. The HPLC/MS data were collected using an Agilent 1100 system coupled to an Agilent 6110 single-quadrupole MS system. The HPLC/MS method used a Grace Prevail RP-C18 column (150 mm × 2.1 mm; particle size = 3 μm). Preparative HPLC was performed using a Waters Delta 600 system equipped with a Waters 996 photodiode-array detector. The Preparative HPLC used a Phenomenex Luna C18 column (150 mm × 21.20 mm; particle size = 5 μm). Melting points were determined using a Reichert−Jung Thermovar apparatus and were uncorrected.

Photophysical Measurements. For photophysical measurements, 2×10^{-5} or 10^{-4} M aqueous solutions of **Ru(Gd.8)$_3$** were used. Absorption spectra were measured on a UVIKON XL spectrophotometer from Secomam using quartz Suprasil cells (Hellma 105.202-QS, bandpass = 1 cm). For collecting luminescence data, samples were placed into 2.4-mm-i.d. quartz capillaries. Emission and excitation spectra were measured on a Horiba−Jobin−Yvon Fluorolog 3 spectrofluorimeter equipped with visible (220−800 nm, a photon-counting unit) and near-infrared (800−1600 nm, a DSS-IGA020L Jobin−Yvon solid-state InGaAs detector cooled to 77 K) detectors. All spectra were corrected for the instrumental functions (excitation and emission). Luminescence lifetimes of Ru^{II} emission were determined under an excitation at 355 nm provided by a YG 980 Quantel Nd:YAG laser equipped with a frequency tripler. The output signal from the visible detector was fed to a Tektronix TDS 754D 500 MHz bandpass digital oscilloscope and then transferred to a personal computer (PC). Lifetimes are averages of at least three independent measurements. Quantum yield was determined with a Fluorolog 3 spectrofluorimeter under excitation into Ru^{II} MLCT band at 450 nm, according to an absolute method using an integration sphere (GMP SA). Each sample was measured several times under slightly different experimental conditions. Estimated experimental error for determination of the quantum yields is 10%−20%. Luminescence images of solutions in capillaries were obtained with Nikon AZ-100 multizoom macroscope equipped with a Photometrics Evolve 512 camera.

^{17}O NMR. ^{17}O NMR measurements of solutions were performed at 11.75 T on 350 μL samples contained in 5-mm-o.d. tubes on a Bruker Avance 500 spectrometer. Temperature was regulated by air or nitrogen flow controlled by a Bruker BVT 3200 unit. ^{17}O transverse relaxation times of distilled water (pH 6.5−7) were measured using a CPMG sequence and a subsequent two-parameter fit of the data points. The 90° and 180° pulse lengths were 27.5 and 55 μs, respectively. The ^{17}O T_2 of water in complex solution was obtained from line-width measurements. All spectra were proton-decoupled. The concentration of the samples was lower than 25 mM. The data are presented as the reduced transverse relaxation rate,

$$\frac{1}{T_2^R} = \frac{55.55}{[\text{Gd complex}]qT_2^P}$$

where [Gd complex] is the molar concentration of the complex, q is the number of coordinated water molecules and T_2^P is the paramagnetic transverse relaxation rate. The sample concentration was determined by ICP-MS and was further confirmed by ^1H relaxometry of a decomplexed sample.

Proton NMRD. Proton nuclear magnetic relaxation dispersion (NMRD) profiles were measured on a Stelar Spinmaster FFC fast field cycling NMR relaxometer over a magnetic field range from 0.24 mT to 1.0 T. Measurements were performed on 0.6 mL samples contained in 10-mm-o.d. Pyrex tubes. Additional relaxation rates at 20 and 60 MHz were obtained on a Minispec mq20 and a Minispec mq60, respectively.

Interaction with HSA. The binding constant and relaxivity value of Gd complexes in a 4% solution of HSA was determined by measuring the proton longitudinal relaxation rate at 20 MHz and 310 K as a function of the concentration of the Gd complex.

Culture and Stimulation of Jurkat T Lymphocytes. Jurkat cells (a gift from Prof. Oberdan Leo, Free University of Brussels, IBMM, Gosselies, Belgium) were cultured at a concentration of 1×10^6 mL^{-1} in RPMI 1640 medium supplemented with 10% NCS (Newborn Calf Serum) and 1% antibiotic−antimicotic. Jurkat cells were stimulated (<10^6 cells/mL, 37 °C, 3 h) with 50 nM PMA (phorbol-12-myristate-13-acetate) to overexpress α_v integrins.[47]

***In Vitro* Validation of Integrin Binding by Proton Relaxometry and T_1-Weighted MRI.** Jurkat cells (2×10^6/mL) were incubated (2 h, ambient temperature) with contrast agents (**Ru(Gd.8)$_3$** or Gd-DOTA) at a concentration of 275 μM. After rinsing three times with TBS buffer (50 mM Tris-HCl, 150 mM NaCl, 1 mM $CaCl_2$, 1 mM $MgCl_2$, 10 mM Hepes, pH 7.4), the cells (7×10^6/0.1 mL) were included in 2% gelatin prepared in PBS. MRI images of cell samples were acquired at 15 °C on a 300 MHz (7 T) Bruker Biospec imaging system (Bruker, Ettlingen, Germany) equipped with a Pharmascan horizontal magnet. For T_1 measurement, we used RARE-T_1 map sequence (T_R: 117.6−10000 ms; number of experiments = 8; T_E = 14.5 ms, slice thickness = 1 mm; FOV = 3 cm; RARE Factor = 2; matrix = 256 × 256; spatial resolution = 117 μm; total time scan = 33 min). The images shown in the figures were acquired with T_1 (T_R = 300 ms, effective echo time = 17 ms, RARE factor = 2, NEX = 10, matrix = 256 × 256, FOV = 3 cm × 3 cm, slice thickness = 1 mm, spatial resolution = 117 μm, TA = 6 min) weighted RARE imaging protocol.

■ ASSOCIATED CONTENT

Ⓢ Supporting Information

The synthesis of ligand **6** (Scheme S1) and complexes **Ln.6** (Scheme S2), as well as the synthetical procedures of **3**, **5**, **6**, **La.6**, **Gd.6**, **Ru(La.6)$_3$**, and **Ru(Gd.6)$_3$**. An HSA titration of **Ru(Gd.8)$_3$** (Figure S1) and an NMRD profile of **Ru(Gd.8)$_3$**, in the presence of 4% HSA (Figure S2). This material is available free of charge via the Internet at http://pubs.acs.org.

■ AUTHOR INFORMATION

Corresponding Author

*E-mail: wim.deborggraeve@chem.kuleuven.be.

Present Address

[‖]Institut des Sciences Moléculaires, Groupe Nanostructures Organiques, UMR 5255 CNRS/Université Bordeaux 1, 351, Cours de la Libération, 33405 Talence Cedex, France.

Notes

The authors declare no competing financial interest.

■ ACKNOWLEDGMENTS

P.V. acknowledges the IWT Flanders (Belgium) for financial support. S.V.E. thanks FWO-Flanders (Project G.0412.09). L.V.E., C.B., S.L., and R.N.M. thank the FNRS, the ARC program (Contract 05/10 335), the ENCITE program, the EMIL program, the Interuniversitary Attraction Poles P6/29 of

the Belgian Federal Science Policy Office, the COST Action D38 and the Center for Microscopy and Molecular Imaging (CMMI, supported by the European Regional Development Fund and the Walloon Region). S.P. acknowledges support from "La Ligue Contre le Cancer" (France) and the "Institut National de la Santé et de la Recherche Médicale" (INSERM). T.N.P.-V. thanks the FWO-Flanders (for Project Nos. G.0412.09 and KAN2008 1.5.157.08).

REFERENCES

(1) Constable, E. C.; Eich, O.; Fenske, D.; Housecroft, C. E.; Johnston, L. A. *Chem.—Eur. J.* **2000**, *6*, 4364−4370.
(2) Jacques, V.; Desreux, J. In *Contrast Agents I*; Krause, W., Ed.; Springer: Berlin/Heidelberg: 2002; Vol. *221*, pp 123−164.
(3) Costa, J.; Ruloff, R.; Burai, L.; Helm, L.; Merbach, A. E. *J. Am. Chem. Soc.* **2005**, *127*, 5147−5157.
(4) Livramento, J. B.; Sour, A.; Borel, A.; Merbach, A. E.; Tóth, É. *Chem.—Eur. J.* **2006**, *12*, 989−1003.
(5) Livramento, J. B.; Weidensteiner, C.; Prata, M. I. M.; Allegrini, P. R.; Geraldes, C. F. G. C.; Helm, L.; Kneuer, R.; Merbach, A. E.; Santos, A. C.; Schmidt, P.; Tóth, É. *Contrast Media Mol. Imaging* **2006**, *1*, 30−39.
(6) Parac-Vogt, T. N.; Elst, L. V.; Kimpe, K.; Laurent, S.; Burtea, C.; Chen, F.; Van Deun, R.; Ni, Y. C.; Muller, R. N.; Binnemans, K. *Contrast Media Mol. Imaging* **2006**, *1*, 267−278.
(7) Paris, J.; Gameiro, C.; Humblet, V.; Mohapatra, P. K.; Jacques, V.; Desreux, J. F. *Inorg. Chem.* **2006**, *45*, 5092−5102.
(8) Moriggi, L.; Aebischer, A.; Cannizzo, C.; Sour, A.; Borel, A.; Bünzli, J.-C. G.; Helm, L. *Dalton Trans.* **2009**, 2088−2095.
(9) Dehaen, G.; Verwilst, P.; Eliseeva, S. V.; Laurent, S.; Vander Elst, L.; Muller, R. N.; De Borggraeve, W. M.; Binnemans, K.; Parac-Vogt, T. N. *Inorg. Chem.* **2011**, *50*, 10005−10014.
(10) Dehaen, G.; Eliseeva, S. V.; Kimpe, K.; Laurent, S.; Vander Elst, L.; Muller, R. N.; Dehaen, W.; Binnemans, K.; Parac-Vogt, T. N. *Chem.—Eur. J.* **2012**, *18*, 293−302.
(11) Kalyanasundaram, K. *Coord. Chem. Rev.* **1982**, *46*, 159−244.
(12) Juris, A.; Balzani, V.; Barigelletti, F.; Campagna, S.; Belser, P.; von Zelewsky, A. *Coord. Chem. Rev.* **1988**, *84*, 85−277.
(13) Aime, S.; Barge, A.; Cabella, C.; Crich, S. G.; Gianolio, E. *Curr. Pharm. Biotechnol.* **2004**, *5*, 509−518.
(14) Beeby, A.; Botchway, S. W.; Clarkson, I. M.; Faulkner, S.; Parker, A. W.; Parker, D.; Williams, J. A. *J. Photochem. Photobiol., B* **2000**, *57*, 83−89.
(15) Charbonnière, L. J.; Ziessel, R.; Montalti, M.; Prodi, L.; Zaccheroni, N.; Boehme, C.; Wipff, G. *J. Am. Chem. Soc.* **2002**, *124*, 7779−7788.
(16) Koullourou, T.; Natrajan, L. S.; Bhavsar, H.; Pope, S. J.; Feng, J.; Narvainen, J.; Shaw, R.; Scales, E.; Kauppinen, R.; Kenwright, A. M.; Faulkner, S. *J. Am. Chem. Soc.* **2008**, *130*, 2178−2179.
(17) Bonnet, C. S.; Tóth, É. *C. R. Chim.* **2010**, *13*, 700−714.
(18) Louie, A. *Chem. Rev.* **2010**, *110*, 3146−3195.
(19) Tallec, G.; Fries, P. H.; Imbert, D.; Mazzanti, M. *Inorg. Chem.* **2011**, *50*, 7943−7945.
(20) Bonnet, C. S.; Buron, F.; Caillé, F.; Shade, C. M.; Drahoš, B.; Pellegatti, L.; Zhang, J.; Villette, S.; Helm, L.; Pichon, C.; Suzenet, F.; Petoud, S.; Tóth, É. *Chem.—Eur. J.* **2012**, *18*, 1419−1431.
(21) Burtea, C.; Laurent, S.; Murariu, O.; Rattat, D.; Toubeau, G.; Verbruggen, A.; Vansthertem, D.; Elst, L. V.; Muller, R. N. *Cardiovasc. Res.* **2008**, *78*, 148−157.
(22) Park, J. A.; Lee, J. J.; Jung, J. C.; Yu, D. Y.; Oh, C.; Ha, S.; Kim, T. J.; Chang, Y. M. *ChemBioChem* **2008**, *9*, 2811−2813.
(23) Verwilst, P.; Eliseeva, S. V.; Carron, S.; Vander Elst, L.; Burtea, C.; Dehaen, G.; Laurent, S.; Binnemans, K.; Muller, R. N.; Parac-Vogt, T. N.; De Borggraeve, W. M. *Eur. J. Inorg. Chem.* **2011**, *2011*, 3577−3585.
(24) Hoshiga, M.; Alpers, C. E.; Smith, L. L.; Giachelli, C. M.; Schwartz, S. M. *Circ. Res.* **1995**, *77*, 1129−1135.
(25) Cai, W.; Niu, G.; Chen, X. *Curr. Pharm. Des.* **2008**, *14*, 2943−2973.
(26) Garanger, E.; Boturyn, D.; Dumy, P. *Anticancer Agents Med. Chem.* **2007**, *7*, 552−558.
(27) Neeman, M.; Gilad, A. A.; Dafni, H.; Cohen, B. *J. Magn. Reson. Imag.* **2007**, *25*, 1−12.
(28) Hirayama, T.; Taki, M.; Kodan, A.; Kato, H.; Yamamoto, Y. *Chem. Commun.* **2009**, 3196−3198.
(29) Pokorski, J. K.; Miller Jenkins, L. M.; Feng, H.; Durell, S. R.; Bai, Y.; Appella, D. H. *Org. Lett.* **2007**, *9*, 2381−2383.
(30) Onishi, H.; Sekine, K. *Talanta* **1972**, *19*, 473−478.
(31) Dijkgraaf, I.; Rijnders, A. Y.; Soede, A.; Dechesne, A. C.; van Esse, G. W.; Brouwer, A. J.; Corstens, F. H. M.; Boerman, O. C.; Rijkers, D. T. S.; Liskamp, R. M. J. *Org. Biomol. Chem.* **2007**, *5*, 935−944.
(32) Rostovtsev, V. V.; Green, L. G.; Fokin, V. V.; Sharpless, K. B. *Angew. Chem., Int. Ed.* **2002**, *41*, 2596−2599.
(33) Tornøe, C. W.; Christensen, C.; Meldal, M. *J. Org. Chem.* **2002**, *67*, 3057−3064.
(34) Muller, R. N.; Raduchel, B.; Laurent, S.; Platzek, J.; Pierart, C.; Mareski, P.; Vander Elst, L. *Eur. J. Inorg. Chem.* **1999**, 1949−1955.
(35) Laurent, S.; Houze, L. V.; Guerit, N.; Muller, R. N. *Helv. Chim. Acta* **2000**, *83*, 394−406.
(36) Botteman, F.; Nicolle, G. M.; Vander Elst, L.; Laurent, S.; Merbach, A. E.; Muller, R. N. *Eur. J. Inorg. Chem.* **2002**, 2686−2693.
(37) Micskei, K.; Powell, D. H.; Helm, L.; Brucher, E.; Merbach, A. E. *Magn. Reson. Chem.* **1993**, *31*, 1011−1020.
(38) Laurent, S.; Vander Elst, L.; Muller, R. N. *Contrast Media Mol. Imaging* **2006**, *1*, 128−137.
(39) Vander Elst, L.; Maton, F.; Laurent, S.; Seghi, F.; Chapelle, F.; Muller, R. N. *Magn. Reson. Med.* **1997**, *38*, 604−614.
(40) Tei, L.; Barge, A.; Crich, S. G.; Pagliarin, R.; Negri, V.; Ramella, D.; Cravotto, G.; Aime, S. *Chem.—Eur. J.* **2010**, *16*, 8080−8087.
(41) Caravan, P.; Ellison, J. J.; McMurry, T. J.; Lauffer, R. B. *Chem. Rev.* **1999**, *99*, 2293−2352.
(42) Solomon, I. *Phys. Rev.* **1955**, *99*, 559.
(43) Bloembergen, N. *J. Chem. Phys.* **1957**, *27*, 572−573.
(44) Freed, J. H. *J. Chem. Phys.* **1978**, *68*, 4034−4037.
(45) Vander Elst, L.; Sessoye, A.; Laurent, S.; Muller, R. N. *Helv. Chim. Acta* **2005**, *88*, 574−587.
(46) Dwek, R. A. In *Nuclear Magnetic Resonance in Biochemistry, Applications to Enzyme Systems*; Clarendon Press: Oxford, 1973; pp 174−283.
(47) Huang, S.; Endo, R. I.; Nemerow, G. R. *J. Virol.* **1995**, *69*, 2257−2263.